Muon Spin Relaxation Study of Spinel Lithium Manganese Oxides

María J. Ariza,*,†,‖ Deborah J. Jones,† Jacques Rozière,† James S. Lord,‡ and Didier Ravot§

Laboratoire des Agrégats Moléculaires et Matériaux Inorganiques UMR CNRS 5072, Université Montpellier II, Place Eugène Bataillon, 34095 Montpellier Cédex 5, France, ISIS Pulsed Muon Facility, Rutherford Appleton Laboratory, Chilton, Oxfordshire OX11 0QX, United Kingdom, Laboratoire de Physicochimie de la Matière Condensée UMR CNRS 5617, Université Montpellier II, Place Eugène Bataillon, 34095 Montpellier Cédex 5, France

Received: September 18, 2002; In Final Form: January 29, 2003

The muon spin relaxation technique has been used to study spinel lithium manganate insertion compounds. Two spinel compositions of lithium manganese oxide have been studied: mixed valence (Mn^{III}/Mn^{IV}) $LiMn_2O_4$, where the lithium extraction process is mainly by redox reaction, and $Li_{1.33}Mn_{1.67}O_4$, where all the manganese is Mn^{IV} and lithium extraction is a lithium by proton ion exchange. Extraction of lithium from the former gives a spinel manganese oxide without lithium or protons (λ-MnO_2), while from the latter a protonated manganese oxide is obtained (H^+-MnO_2). Muons are quasi-static in these compounds, and they are located both in "regular" lithium and proton sites and in interstitial sites of the spinel structure, these latter being used during diffusion of lithium ions and protons. Results clearly reflect the presence of protons in H^+-MnO_2 and the movement of lithium ions in both lithium manganates. The lithium-rich phase $Li_{1.33}Mn_{1.67}O_4$ is characterized by an increase of the number of implanted muons localized in interstitial sites, as well as by a decrease of the onset temperature for lithium diffusion.

1. Introduction

Spinel manganese oxides are three-dimensional insertion compounds with a high specificity for lithium ions. They have been studied extensively both as cathode materials for lithium batteries and as materials for lithium extraction from aqueous solutions.[1−11] λ-MnO_2 is a metastable oxide obtained by removing Li ions from the ideal spinel $LiMn_2O_4$. Lithium extraction can be achieved either chemically by aqueous acid treatment or electrochemically in nonaqueous cells,[2,4,12] and it leads to materials that maintain the cubic spinel symmetry (space group $Fd\bar{3}m$) of composition $Li_x[Mn_{2-y}Li_y]O_4$. x refers to the occupation of regular tetrahedral Li 8a sites, and it ranges between 0.2 (charged state) and 1 (empty state) in lithium battery applications, while y takes into account the amount of extra Li atoms. This extra lithium has been localized substituting Mn in octahedral 16d sites by neutron diffraction.[9,13] Li substitution increases the mean Mn valency up to the point at which only Mn^{IV} is present, theoretically for $y = 0.33$. In consequence, it reduces the structural phase transition that $LiMn_2O_4$ undergoes at ∼290 K due to the presence of 50% of the Jahn−Teller ion Mn^{III},[14] which leads to reduced charge/discharge cycling battery performance. On the other hand, an excess of lithium has been shown to reduce the capacity of the spinel to approximately $148(1 - 3y)$ mA h/g.[15] Of a number of neutron diffraction studies, one has shown the presence of Li atoms in interstitial octahedral 16c sites for $Li_{1.28}Mn_{1.72}O_4$.[16] Thus, y must be small ($0.04 \leq y \leq 0.06$) for optimal battery performance.

The mechanism of the lithium sorption reaction depends on the amount of Mn^{IV} in the spinel: for $LiMn_2O_4$ ($Mn^{III}/Mn^{IV} = 1$), lithium extraction has been shown to be predominantly a redox reaction (Mn^{III} to Mn^{IV}), while for $Li_{1.33}Mn_{1.67}O_4$ ($Mn^{III}/Mn^{IV} = 0$) this reaction involves essentially a lithium by proton ion exchange process.[7,9] The high hydrogen content of spinel manganese oxides obtained from a lithium manganate precursor with high manganese oxidation state has also attracted attention to their properties as protonic oxides.[17] Here, protonic species have been identified by inelastic neutron scattering (INS) as hydroxyl ions and lattice water associated with octahedral manganese vacancies.[17] The hydroxyl protons have been located by neutron diffraction in 96g sites, at 1.1 Å from oxygen adjacent to Mn vacancies,[9] and they are eliminated during lithium sorption while water molecules remain trapped in the spinel lattice.[17] The lithium insertion/deinsertion process in rechargeable Li ion cells is performed in a nonaqueous environment. However, a certain degree of nonreversibility of proton insertion in spinel lithium manganates could be one of the reasons for capacity fading,[18] but the presence and nature of inserted protons is extremely difficult to follow due to the very low hydrogen concentration.[19] Not only the presence of protons but also their dynamic properties, as well as a possible correlation between diffusion of protons and Li ions, is of fundamental importance for developing lithium manganates with batteries and ion exchange applications.

For lithium-rich manganate spinels ($y > 0.13$), ab initio band structure calculations have shown energy differences between vacant 16d Mn and interstitial 16c sites to be small.[20] Thus, it is believed that diffusing Li ions pass through 16c sites before localizing in 16d sites for battery materials (low y), but protons

* Corresponding author. Fax: +34 968 325932. E-mail: mj.ariza@upct.es.
† Laboratoire des Agrégats Moléculaires et Matériaux Inorganiques UMR CNRS 5072, Université Montpellier II.
‡ Rutherford Appleton Laboratory.
§ Laboratoire de Physicochimie de la Matière Condensée UMR CNRS 5617, Université Montpellier II.
‖ Present address: Departamento de Arquitectura Técnica, Area de Química Física, Universidad Politécnica de Cartagena, Paseo Alfonso XIII, 30203, Spain.

10.1021/jp027022n CCC: $25.00
Published on Web 05/28/2003

must diffuse by a mechanism involving local distortion of O−H bonds and the hydrogen bond network. However, only very partial information on Li^+ and H^+ ion mobility in this family of spinel lithium manganates can be found in the literature. Lithium dynamics have been studied by ^6Li and ^7Li nuclear magnetic resonance,[21] and recently by zero-field muon spin relaxation (μSR) in $Li_{1.04}Mn_{1.96}O_4$.[22] The μSR technique uses polarized positive muons as a local probe of the magnetic properties of materials and spin dynamics. Muons can be implanted into any material, and the direction of the muon spin at the instant of decay ($\mu^+ \rightarrow e^+ + \nu_e + \bar{\nu}_\mu$, lifetime = 2.179 μs) provides information on the dynamics of the muon during its lifetime and on the static and fluctuating magnetic fields from neighboring nuclear and atomic moments.[23−27] Since the positive muon can be considered as a light proton, it has been used for modeling the diffusion and trapping sites of H^+ in various solids.[28−30] Only a very small number of muons are stopped in the sample at any one time ($\sim 10^2$−10^3 muons), so modeling a material with a very low proton concentration. The high sensitivity allows small amounts of magnetic impurities to be detected.[24] μSR is therefore a technique suitable for the study of the dynamic properties of H^+ and/or Li^+ ions, which is the aim of this work. Moreover, since μSR is a probe technique, both samples containing and not containing Li or H^+ can be studied, which allows the study of proton dynamics and confirms some assumptions derived from previous Li NMR results based only on Li-containing samples.

In the present contribution, we report μSR results on four spinel manganese oxides: $LiMn_2O_4$ ($y = 1$, $x = 0$), $Li_{1.33}Mn_{1.67}O_4$ ($y = 1$, $x = 0.33$), and the two corresponding lithium-extracted samples, denoted λ-MnO_2 and H^+-MnO_2, respectively. Samples were first characterized for their crystal structure and chemical composition, as well as their magnetic properties. General results concerning the μSR experiments are presented in section 3, and in section 4 we discuss and interpret μSR results for each sample according to different models.

2. Experimental Section

Spinel lithium manganese oxides were prepared by a solid-state reaction of stoichiometric amounts of lithium carbonate and manganese carbonate.[7] To obtain $LiMn_2O_4$, the finely ground mixture of the precursors was fired at 800 °C in air for 20 h, while the carbonate mixture for $Li_{1.33}Mn_{1.67}O_4$ was fired at 400 °C in air for 8 h. The lithium extraction process was carried out by stirring these parent samples in 0.2 M HCl for 48 h, after which samples were washed with distilled water and dried at 50 °C for 24 h. For $Li_{1.33}Mn_{1.67}O_4$, this process produces a sample in which protons are exchanged for lithium ions (denoted H^+-MnO_2), while $LiMn_2O_4$ produces a sample containing no lithium or protons (λ-MnO_2). The samples were initially characterized by powder X-ray diffraction (XRD) for phase identification and to assess spinel phase purity. X-ray diffractograms were recorded with 0.02° angular steps and the unit cell parameter (a) was calculated from diffraction angles (θ) associated to eight diffraction planes by using DOPOWDER software. This program gives errors of the cell constant based on the fitting of the experimental peaks to the position corresponding to a cubic spinel crystalline cell. The lithium content of the samples was determined by atomic emission spectrometry of samples dissolved in hydrochloric acid and hydrogen peroxide. Three measurements were performed using fresh samples each time, and in all cases, experimental data dispersion was lower than 10%.

Magnetic measurements were carried out using a vibrating sample magnetometer from Oxford Instruments. Thermal dependence of magnetic susceptibility was measured using a static magnetic field of 0.1 T at increasing temperature from 2 to 300 K after zero-field cooling. Isothermal magnetization curves were obtained from 0.5 to 1 T magnetic field.

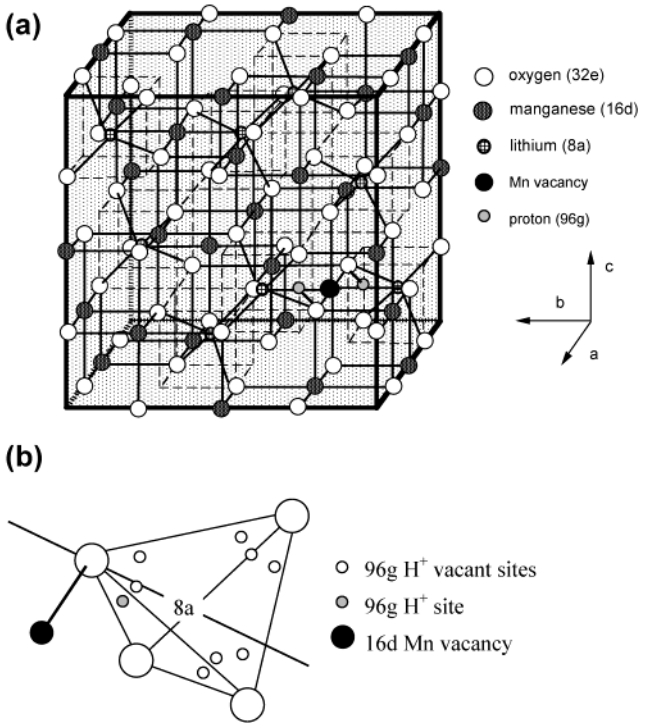

Figure 1. (a) Regular spinel lattice for protonated manganese oxide. (b) Most probable proton sites inside an 8a oxygen tetrahedron.[9]

Zero-field (ZF) muon spin relaxation experiments in the temperature range $100 \leq T \leq 400$ K were performed on the MuSR instrument at the ISIS pulsed muon source (Rutherford Appleton Laboratory, U.K.). About 2 g of the sample was placed in aluminum holders with a window of thin Mylar film. Calibration parameters were determined from a 20 G transverse field (TF) measurement, and longitudinal field (LF) experiments at 50 G were also performed to experimentally determine the muon spin relaxation rate (λ_z) due to paramagnetic manganese.

3. Results

3.1. Structural and Chemical Characterization. The cubic spinel structure (see Figure 1a) of each of the samples was confirmed by powder X-ray diffraction. Figure 2 shows the XRD patterns of the two lithium manganate phases and their lithium-extracted products. All four samples present very similar peak patterns, which correspond to different diffraction planes in the $Fd\bar{3}m$ space group.[31] As indicated by the higher intensity and narrower diffraction lines, $LiMn_2O_4$ and λ-MnO_2 are of higher crystallinity than $Li_{1.33}Mn_{1.67}O_4$, and H^+-MnO_2, and no evidence for Li_2MnO_3 was found in any sample.

Table 1 summarizes the results of structural and chemical characterization, as well as some magnetic parameters. The unit cell parameter (a) for $LiMn_2O_4$ and $Li_{1.33}Mn_{1.67}O_4$ is in the typical range for spinel lithium manganates. In the former, the higher value of a indicates a lower average oxidation state for Mn ($\sim$3.5), while for the latter $a = 8.13$ Å is a value characteristic of samples with higher manganese oxidation state (close to 4).[7] Thus, XRD results suggest the Mn/O ratio is as expected for both parent compounds, which allows writing their empirical formulas by only lithium chemical analysis. Although differences are within the 10% expected experimental errors

TABLE 1: Lattice Constant (*a*) and Li/Mn Atomic Ratio and Chemical Formula of the Two Spinel Lithium Manganates and Their Lithium-Extracted Products[a]

sample	a^b (Å)	Li/Mn[c]	formula[c]	$\mu_{eff}{}^d$ (μ_B)	θ^d (K)
$LiMn_2O_4$	8.24 ± 0.01	0.505	$Li_{1.01}Mn_2O_4$	4.44 ± 0.03	−264 ± 6
λ-MnO_2	8.04 ± 0.01	0.045	$Li_{0.09}Mn_2O_4$	3.78 ± 0.04	−106 ± 8
$Li_{1.33}Mn_{1.67}O_4$	8.14 ± 0.01	0.774	$Li_{1.29}Mn_{1.67}O_4$	3.74 ± 0.02	22 ± 2
H^+-MnO_2	8.04 ± 0.01	0.012	$Li_{0.02}H_{1.31}Mn_{1.67}O_4$	3.95± 0.03	−109 ± 6

[a] Effective magnetic moment (μ_{eff}) and Weiss temperature (θ) obtained from magnetic susceptibility measurements. [b] Errors given by DOPOWDER software. [c] Obtained from Li chemical analysis only. Mn, O, and H contents were fixed to expected values. [d] Errors correspond to standard deviation of four values of these parameters obtained by linear fitting of χ^{-1} (T) in different temperature ranges (from 74, 100, 126, and 150 K to 300 K). Linear regression coefficient better than 0.999 in all cases.

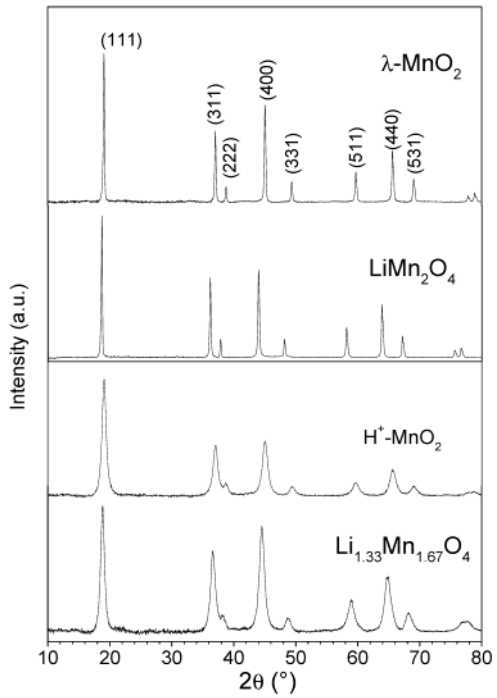

Figure 2. X-ray diffraction patterns of λ-MnO_2, $LiMn_2O_4$, H^+-MnO_2, and $Li_{1.33}Mn_{1.67}O_4$ from top to bottom.

for both samples, the content of lithium in $LiMn_2O_4$ is closer to the expected value than that for $Li_{1.33}Mn_{1.67}O_4$, where it is slightly lower than expected. Previous studies have shown that a Li/Mn ratio higher than 0.75 only can be achieved by a deficiency in oxygen content (see discussion in ref 7). In any case, both structural and chemical analyses have shown that parent samples prepared here correspond to spinel $LiMn_2O_4$ and $Li_{1.33}Mn_{1.67}O_4$.

The chemical extraction process is more effective with $Li_{1.33}Mn_{1.67}O_4$, where only 1.5% of the parent lithium content remains after acid washing to give H^+-MnO_2 versus 9% in λ-MnO_2. As previously shown by neutron diffraction experiments,[9] these small amounts of residual lithium in H^+-MnO_2 are not in 16d sites (manganese vacancies) but are in 8a regular Li sites. Remaining Li has been also attributed to very small amounts of Li_2MnO_3 impurities, not detected by X-ray diffraction.[29] For $Li_{1.33}Mn_{1.67}O_4$, the insertion of protons occurs on 96g sites at ca. 1 Å from oxygen atoms close to a 16d Mn vacancy (see Figure 1b) and, assuming all the manganese are Mn^{IV}, only one proton per 8a Li vacancy can be inserted at most. As expected, the spinel structure is retained in λ-MnO_2 and H^+-MnO_2, and the lithium extraction provokes a decrease of the unit cell parameter (see Table 1).

3.2. Magnetic Properties. Figure 3 shows the thermal evolution of the magnetic susceptibility (χ) per mole of manganese, and the inverse susceptibility (inset), for $LiMn_2O_4$, $Li_{1.33}Mn_{1.67}O_4$, λ-MnO_2, and H^+-MnO_2. For $Li_{1.33}Mn_{1.67}O_4$, χ increases very quickly at low temperature and has a maximum close to $T = 6$ K, which indicates that magnetic ordering could occur suddenly at this temperature. For $T \geq 100$ K, the inverse susceptibility follows a Curie−Weiss law: $\chi = C/(T - \theta)$ in all samples. Linear correlation of the data is better than 0.999 for all samples. Values of the effective magnetic moment (μ_{eff}), obtained from the Curie constant (C), and the Weiss temperature (θ) are also listed in Table 1. Errors have been estimated by fitting the experimental data in different temperature ranges, from 74, 100, 126, and 150 K to 300 K. As can be seen, the Curie−Weiss parameters are independent of the used temperature range, which also gives validity to values in Table 1. Experimental μ_{eff} values for $Li_{1.33}Mn_{1.67}O_4$, H^+-MnO_2, and λ-MnO_2 are very close to the expected value of Mn^{IV} ions in the ground state ($\mu_{eff\,0}(Mn^{IV}) = 3.87\ \mu_B$), while μ_{eff} for $LiMn_2O_4$ agrees with the presence of 50% Mn^{IV} and 50% high-spin Mn^{III} ion ($\mu_{eff\,0}(Mn^{III}) = 4.90\ \mu_B$), as expected for this sample. The θ values are characteristic of a net antiferromagnetic interaction between the Mn spins for all samples except for $Li_{1.33}Mn_{1.67}O_4$, where the extrapolation of the linear law intercepts the positive part of the *x*-axis (see Figure 3). These results agree with those reported previously for both lithiated samples[29,33,34] and for λ-MnO_2.[35] A crossover from antiferromagnetic to ferromagnetic interaction with increasing Mn valence in spinel lithium manganates can be explained by the increase in the number of Mn^{IV}−O−Mn^{IV} 90° bonds (ferromagnetic interaction) relative to Mn^{III}−Mn^{IV} and Mn^{III}−O−Mn^{IV} 90° bonds (antiferromagnetic interaction).[14,34] In contrast, the antiferromagnetic Mn^{IV}−Mn^{IV} interaction dominates the magnetic behavior of λ-MnO_2 and H^+-MnO_2 due to their smaller lattice parameters,[33,34] although the presence of a very small amount of Mn^{III} in these samples could be also responsible for antiferromagnetism, since the next nearest and further Mn^{III}−Mn^{III} interactions are very large and negative.

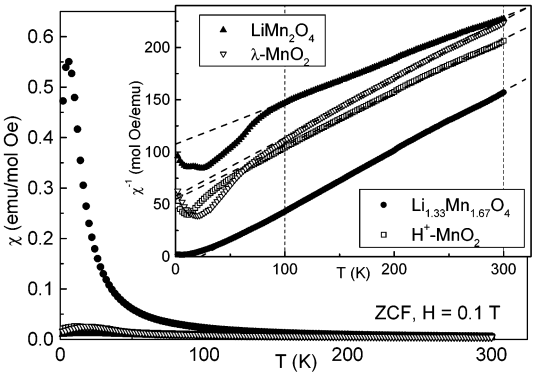

Figure 3. Temperature dependence of magnetization and inverse of the magnetization (inset) for $LiMn_2O_4$, λ-MnO_2, $Li_{1.33}Mn_{1.67}O_4$, and H^+-MnO_2 (zero-field cooling, 0.1 T applied field).

3.3. Muon Spin Relaxation Measurements. Zero-field μSR spectra of $LiMn_2O_4$, λ-MnO_2, $Li_{1.33}Mn_{1.67}O_4$, and H^+-MnO_2 at temperatures between 100 and 400 K are displayed in Figure

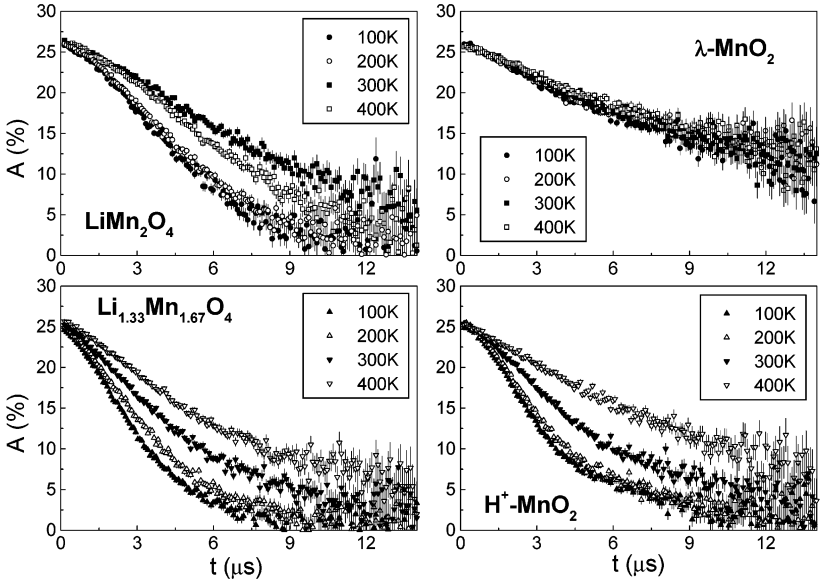

Figure 4. Comparison of ZF μSR spectra at different temperature for $LiMn_2O_4$, λ-MnO_2, $Li_{1.33}Mn_{1.67}O_4$, and H^+-MnO_2.

4. The shape of the spectra is close to Gaussian for temperatures below 200 K in all samples except λ-MnO_2, and a dynamical Kubo−Toyabe function can be used to describe their depolarization over the whole temperature range. The initial asymmetry (A_0) is always close to 0.25 for both ZF and 20 G TF spectra, which indicates full diamagnetic muon fraction as found in metals and many oxides. In addition, transverse runs show oscillations of ~0.27 MHz frequency but also damping with a Lorentzian envelope. This behavior is also characteristic of diamagnetic muons experiencing rapidly fluctuating fields from paramagnetic moment fluctuations.[25]

The paramagnetic fluctuation effect can be taken into account in the relaxation function by an exponential factor characterized by the relaxation rate λ_z. Then, experimental asymmetry ($A_z(t)$) is given by the expression

$$A_z(t) = A_0 P_{KT}(\Delta,\nu,t)e^{-\lambda_z t} \quad (1)$$

where the Kubo−Toyabe function describes interactions with near neighbor nuclei in a zero external field.[23−27] For a low muon hop rate $\nu \ll \Delta$ the Kubo−Toyabe function can be written as

$$P_{KT} = A_0\left(\frac{1}{3}e^{-2\nu t/3}[1 + 2(1 - \Delta^2 t^2)]e^{-\Delta^2 t^2/2}\right)P_{KT}(\Delta,\nu,t)e^{-\lambda_z t} \quad (2)$$

where Δ and ν are the Kubo−Toyabe static muon depolarization rate and the muon hopping rate, respectively. For static muons ($\nu = 0$), the ν exponential factor can be omitted, for larger hop rates the function must be evaluated by integration, and for very large hop rates P_{KT} can be approximated by a simple exponential with relaxation rate inversely proportional to the hop rate. For muons localized in n sites ($n = 2, 3, ...$) with different local magnetic fields, n Kubo−Toyabe functions ($P_{KTi}(\Delta_i,\nu_i,t)$, $i = 1, 2, ..., n$) must be summed.

Experimentally, λ_z can be determined from LF runs at magnetic fields sufficiently large to quench the nuclear depolarization. Figure 5a plots this experimental relaxation rate versus the temperature. Above 100 K, the nuclear relaxation rate was temperature independent for $LiMn_2O_4$, λ-MnO_2, and H^+-MnO_2, while $Li_{1.33}Mn_{1.67}O_4$ has the largest λ_z that decreases by more than 30% between 100 and 350 K. However, the 50 G μSR

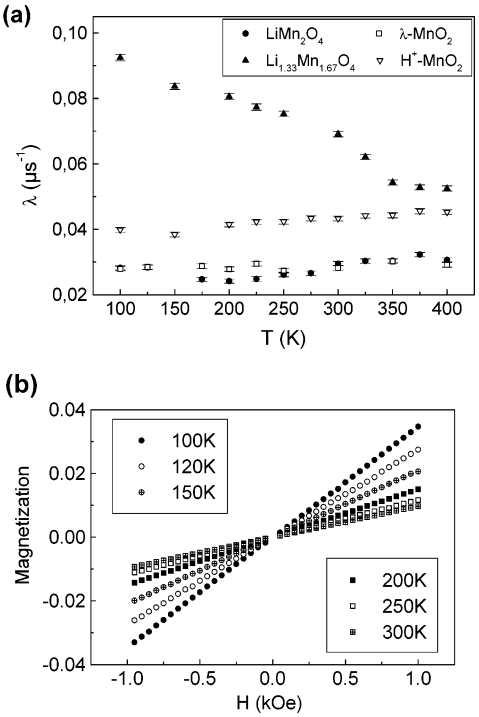

Figure 5. (a) Dependence with temperature of relaxation rate due to the paramagnetic fluctuation effect (λ_z). (b) Magnetization as a function of the applied field H of $Li_{1.33}Mn_{1.67}O_4$ at different temperatures.

spectra show an exponential shape over the whole temperature range. The influence of Mn magnetism on muon relaxation could be the cause of this decrease, since $Li_{1.33}Mn_{1.67}O_4$ also has the largest magnetic susceptibility. In this sample, a small increase of the initial asymmetry also occurs between 300 and 325 K in both TF and ZF spectra. The linearity of χ with the magnetic field up to 0.1 T in this temperature range was also tested with $Li_{1.33}Mn_{1.67}O_4$ (see Figure 5b).

As can be observed in Figure 4, muon depolarization does not significantly change with increasing temperatures for λ-MnO_2, while it becomes weaker for the other three samples. In $LiMn_2O_4$ this trend changes at high temperature and depolarization becomes slightly stronger for $T > 350$ K than for $275 < T \leq 350$ K. Figure 6 compares the μSR spectra of

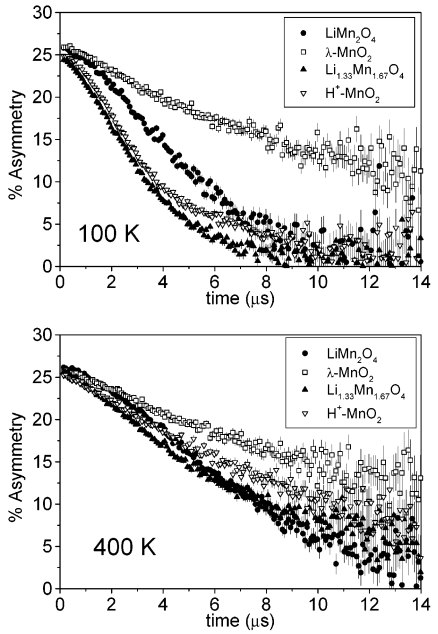

Figure 6. Comparison of ZF μSR spectra of $LiMn_2O_4$, λ-MnO_2, $Li_{1.33}Mn_{1.67}O_4$, and H^+-MnO_2 at 100 (top) and 400 K (bottom).

the four samples at 100 K; $Li_{1.33}Mn_{1.67}O_4$ shows stronger depolarization than $LiMn_2O_4$, and both lithium-extracted samples present less depolarization than their parent compounds. On the other hand, the shape of the H^+-MnO_2 spectrum at 100 K shows two Gaussian components, which indicates the existence of at least two different depolarization rates that can be due to muons at two different muon sites. Indeed, in the other samples muons may also go into two different sites but with very similar depolarization rates, while the presence of protons nearby gives two different values of depolarization in H^+-MnO_2. Here, therefore, a model in which all muons relax in the same way (one-site model) and other one in which the spin relaxes in two different ways (two-site model) may be used to approach spectral interpretation.

3.3.1. One Muon Site Model. The μSR spectra of $LiMn_2O_4$, λ-MnO_2, and $Li_{1.33}Mn_{1.67}O_4$ can all be well fitted with one Kubo−Toyabe component (eq 1) over the whole temperature range. A fit of H^+-MnO_2 spectra can also be performed, although agreement between experimental and calculated data is better using two components, especially at low temperatures (see Figure 7b). The dependence of the static line width (Δ) and the muon hopping rate (ν) with temperature is shown in parts a and b, respectively, of Figure 8. A drop of the KT line width occurs in $LiMn_2O_4$ at ~250 K, while for $Li_{1.33}Mn_{1.67}O_4$ the decrease begins around 150 K. This behavior is similar to that previously reported for $Li_{1.04}Mn_{1.96}O_4$,[22] where the onset of the decrease in line width was observed around 230 K. As concluded also for $Li_{1.04}Mn_{1.96}O_4$, the thermal dependence of Δ in samples containing lithium cannot be due to a muon diffusion effect, since ν is quite constant over all the temperature range and the asymmetry spectra always present a parabolic shape at short times. This thermal dependence can only be understood by assuming that the contribution of Li^+ ions to muon depolarization is motionally narrowed when some lithium ions diffuse. Experimentally, this assumption is supported by the invariability of Δ with temperature in the corresponding lithium-extracted, proton-free sample; i.e., the average value of Δ in the whole temperature range is $0.131 \pm 0.007\ \mu s^{-1}$ for λ-MnO_2. Therefore, these results indicate that the temperature for onset of Li^+ ion diffusion decreases with an increase in the amount of lithium in the spinel manganese oxide, which is not incompatible with a higher Li^+ diffusion coefficient on $LiMn_2O_4$ than on $Li_{1.33}Mn_{1.67}O_4$ found from NMR experiments,[21] since NMR data will average over all Li nuclei whereas muons only interact with those Li nearest to the muon. Because the muon is simulating a proton, the Li^+ ions nearest it are in sites not typical of H^+-free lithium manganese oxides.

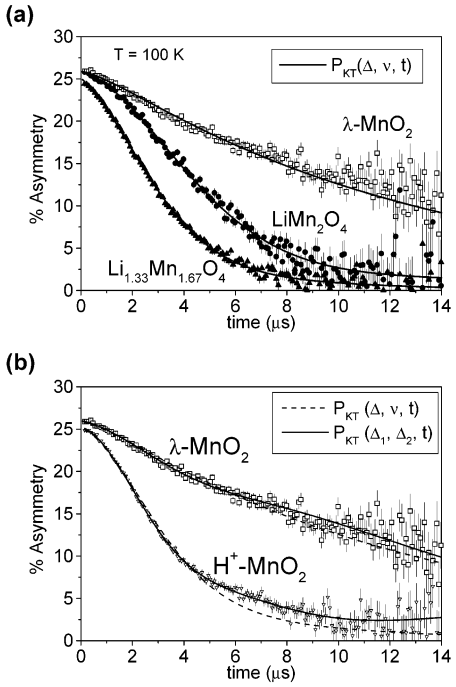

Figure 7. (a) Comparison of 100 K experimental ZF μSR spectra of λ-MnO_2, $LiMn_2O_4$, $Li_{1.33}Mn_{1.67}O_4$, and the fitted spectra by the one muon site model. (b) Comparison of the experimental, the one site, and the two-site fitted μSR spectra for λ-MnO_2 and H^+-MnO_2 at 100 K.

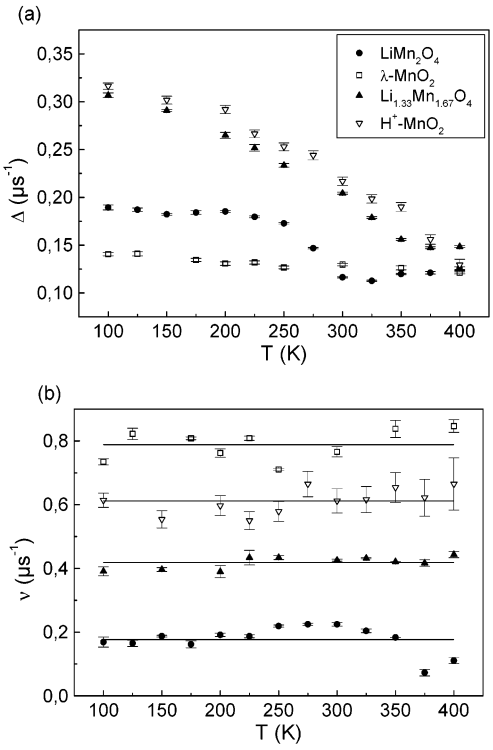

Figure 8. Thermal dependence of one muon site model parameters. (a) Static line width (Δ); (b) muon hopping rate (ν).

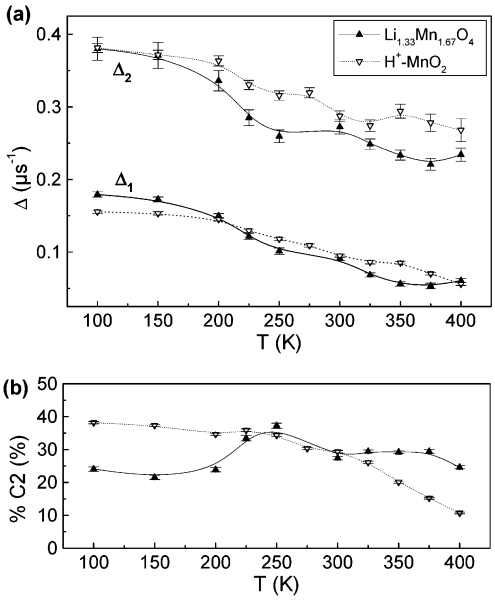

Figure 9. Thermal dependence of two muon site static model parameters for $Li_{1.33}Mn_{1.67}O_4$ and H^+-MnO_2. (a) Static line widths (Δ_1 and Δ_2); (b) relative intensity of component 2 (% C2).

At low temperature, Δ is much higher for H^+-MnO_2 than for λ-MnO_2, due to the presence of H^+. On the other hand, the muon hopping rate is very similar for $LiMn_2O_4$ and for $Li_{1.04}Mn_{1.96}O_4$,[22] but it increases in $Li_{1.33}Mn_{1.67}O_4$ and for both lithium-extracted samples. The latter parameter takes into account muon fluctuations and also fluctuations in Mn spin, and depends largely on the Mn−Mn spin coupling, and it is to be expected that all samples containing Mn^{IV} present large ν values.

3.3.2. Two Muon Site Model. As can be observed in Figure 7b, H^+-MnO_2 asymmetry spectra are better reproduced by including two static Kubo−Toyabe components in the fitting process ($P_{KT}(\Delta_1,t)$ plus $P_{KT}(\Delta_2,t)$). For comparison, all samples were fitted in this way, and later we discuss the validity of this two-site model and equivalences between both models. For the two-site model, fitting parameters are the initial asymmetry (A_0), the two line widths (Δ_1 and Δ_2), and the relative intensity between components. A depolarization rate of magnetic origin (λ_z) was assumed to be the same for both muon sites. Parts a and b, respectively, of Figure 9 show the dependence on temperature of both line widths and the relative percentage of muons in "site 2". For $Li_{1.33}Mn_{1.67}O_4$ and H^+-MnO_2 both line widths decrease when temperature increases.

4. Interpretation and Discussion of μSR Results

For these samples, in which the muon spectra have roughly a Gaussian shape, the field distribution at the muon site can be expressed as a lattice sum over Mn, Li, and H nuclear magnetic moments. If both muons and nuclei are static and the effect of the electric field gradient on the nuclear quadrupole moments is neglected, the field depends only on the muon to atom distances and the nuclear moment values, and thus, Δ can be computed for a given muon site if positions of the magnetic nuclei are known.[36] Although, even at low temperatures, atomic positions in these insertion materials are not exactly known, an approach can be made by assuming different configurations or "ideal structures". For $LiMn_2O_4$, all regular 8a sites in the $Fd\bar{3}m$ space group must be occupied by Li, 16d by Mn, and 32e by O atoms, but only Li and Mn nuclei contribute to the line width. The situation is identical for λ-MnO_2 but without Li nuclei. For the lithium-rich sample, Li is mostly in 8a and in vacant 16d manganese sites.[9] H^+-MnO_2 is the most complicated situation, since not only Mn, but also the nuclear moment of the protons, contributes to the Δ value (Li atoms were not considered since the amount of lithium remaining in the sample is lower than one atom per unit cell). According to neutron diffraction experiments, protons lie in 96g sites in the space defined by oxygen tetrahedra at ∼1 Å from oxygen atoms and at ∼2.45 Å from vacant Mn sites.[9,37] Taking all information into account, line width values were calculated using atomic configurations with different vacant sites and substitutional atoms. A wide variety of muon sites were tested for each configuration, including regular H, Li, and Mn sites since even in the highly crystallized $LiMn_2O_4$ the amount of defect sites may be higher than the amount of muons (less than 10^3 muons implanted on about 10^{20} spinel unit cells). Different ideal structures have been named taking into account the number and type of nuclear moments which contribute to Δ (16Mn8Li for ideal $LiMn_2O_4$). Calculated line width values (Δ_{th}) using the cell parameters of Table 1 with and without a lithium contribution are summarized in Table 2 for $LiMn_2O_4$ and $Li_{1.33}Mn_{1.67}O_4$. Line width values for ideal λ-MnO_2 may be similar to those listed in the column "16Mn", since an increase less than 7.7% is expected for the small lattice contraction ($\Delta \propto r^{-3}$). In contrast, the electric field gradient effect on the nuclear moments can reduce calculated line width values (∼15% at most).[22] For H^+-MnO_2, the field is different at structurally equivalent sites due to the presence of protons. Table 3 lists some of the most relevant calculated line width values for that sample. In some cases, several Δ_i values of equivalent sites have been averaged assuming the same probability for all of them and taking into account that the total line width can be written as $\Delta^2 = \sum_i p_i \Delta_i^2$, where p_i is the relative muon occupancy of site i. Numbers in bold are the multiplicity of averaged equivalent sites. Finally, it should be remembered that Δ values calculated in this way are only comparable to Δ obtained from a Kubo−Toyabe fitting of zero-field μSR data; therefore, fitted Δ values obtained from both the one- and two-site models can be compared with these calculated line widths.

At low temperature, static conditions of the atoms are better satisfied and experimental Δ values can be compared with calculated Δ_{th} values. At the fast movement limit of lithium atoms, their contribution to the line width decreases and disappears at high temperature. In contrast, if there is a strong correlation between the muon and the Li^+ ions, muons may act as a tracer of the Li^+ diffusion. Furthermore, the magnetic moment of the Mn atoms, which causes the additional muon relaxation rate λ_z, also interacts with the other nuclei. For Li and H this can usually be neglected, but the Mn nuclei interact much more strongly with their own atomic moment, with a relaxation rate perhaps 100 times that of the muon. This may give an effect similar to motional narrowing of the relaxation due to Mn−Mn interaction.

4.1. $LiMn_2O_4$. According to the one muon site model, $\Delta = 0.19\ \mu s^{-1}$ for $LiMn_2O_4$ at low temperature. This value can be explained if muons are mostly in vacant 8a sites and a small amount (∼10%) in 16c sites. If an 8a Li site is vacant, Δ_{th} at 96g sites is only slightly higher than at the 8a site (see Table 2). Moreover, the motion of muons around the three equivalent 96g sites for each of the four oxygens could reduce this value, such that the average local field felt by quasi-static muons in 96g sites could be quite similar to that experienced by static muons in 8a sites. Therefore, these results do not exclude the presence of muons at ∼1 Å from oxygen atoms. Results

TABLE 2: Calculated Δ Values at Different Muon Sites for $LiMn_2O_4$ (16Mn8Li) and $Li_{1.33}Mn_{1.67}O_4$ (between 13Mn11Li and 14Mn10Li) Ideal Samples[a]

μ-site Wyckoff: coord	calculated Δ_i values (μs^{-1})					
	16Mn8Li	16Mn	14Mn10Li	14Mn	13Mn11Li	13Mn
8a: (1/8 1/8 1/8)	0.15	0.14	0.16	0.13	0.16	0.12
16d: (1/2 1/2 1/2)	0.18	0.17	0.19	0.15	0.19	0.15
96g:(0.184 0.152 0.162)	Li[b]	0.16	Li[b]	0.13	Li[b]	0.13
(1/2 3/8 1/8)	0.52	0.53	0.54	0.16	0.54	0.16
(3/8 1/4 1/8)	0.52	0.53	0.54	0.16	0.54	0.16
(7/8 3/4 7/8)	1.32	0.18	1.37	0.17	1.37	0.17
(0 7/8 7/8)	1.32	0.18	1.37	0.17	1.37	0.16
48f: (1/2 7/8 7/8)	0.68	0.73	0.70	0.70	0.71	0.70
(5/8 3/4 7/8)	0.52	0.53	0.54	0.51	0.54	0.51
(1/4 1/8 1/8)	1.32	0.18	1.36	0.15	1.36	0.14
(1/8 0 1/8)	1.32	0.18	1.36	0.15	1.36	0.14
16c: (0 0 0)	0.39	0.17	0.41	0.15	0.41	0.14
8b: (3/8 3/8 3/8)	0.52	0.55	0.41	0.46	0.54	0.46

[a] Values without the Li contribution are also listed. λ-MnO_2 sample ideally corresponds approximately to the 16Mn column. Since vacancy can occur, regular H, Li, Mn, and O sites are probed as well as interstitial sites. [b] Muon positions extremely close to a Li atom, not physically meaningful within the ionic radius.

TABLE 3: Calculated Δ Values at Different Muon Sites for H^+-MnO_2[a]

μ-site Wyckoff: coord	calculated Δ_i values (μs^{-1})					
	13Mn6H	13Mn7H	13Mn8H	14Mn4H	12Mn8H	12Mn
8a: (1/8 1/8 1/8)	H[b] **3**	H[b] **4**	H[b] **4**	H[b] **2**	H[b] **4**	0.13 **8**
(3/8 7/8 3/8)	H[b] **3**	H[b] **3**	H[b] **4**	H[b] **2**	H[b] **4**	
(7/8 7/8 7/8)	0.16 **2**	0.16 **1**		0.15 **4**		
16d: (1/2 1/2 1/2)	0.19 **16**	0.19 **16**	0.20 **16**	0.18 **16**	0.20 **16**	0.15 **16**
96g: H^+	0.16	0.17	0.17	0.16	0.17	0.13
vacant H^+	1.30	1.30	1.30	1.30	1.30	0.14
(1/2 3/8 1/8)	0.23	0.23	0.23	0.54	0.23	0.17
(3/8 1/4 1/8)	0.38	0.38	0.39	0.62	0.39	0.17
(7/8 3/4 7/8)	0.19	0.20	H[b]	0.19	H[b]	0.17
(0 7/8 7/8)	0.18	0.20	0.49	0.18	0.49	0.17
48f: (1/2 7/8 7/8)	0.73	0.73	0.74	0.73	0.54	0.53
(5/8 3/4 7/8)	0.54	0.54	0.66	0.54	0.43	0.17
(1/4 1/8 1/8)	H[b]	H[b]	H[b]	H[b]	H[b]	0.15
(1/8 0 1/8)	0.72	0.72	0.72	0.72	0.72	0.15
16c: (0 0 0)	0.22 **5**	0.24 **4**	0.25 **4**	0.19 **8**	0.24 **4**	0.14 **12**
(0 1/4 1/4)	0.44 **6**	0.36 **6**	0.46 **4**	0.44 **4**	0.45 **4**	0.16 **4**
(1/4 0 1/4)	0.60 **3**	0.61 **3**	0.61 **4**	0.60 **4**	0.61 **4**	
(1/4 1/4 0)	0.72 **2**	0.72 **3**	0.72 **4**		0.72 **4**	
8b: (1/8 1/8 5/8)	0.49 **6**	0.49 **6**	0.49 **6**	0.49 **6**	0.49 **8**	0.48 **8**
(5/8 5/8 5/8)	0.55 **2**	0.56 **2**	0.56 **2**	0.56 **2**		

[a] Ideal samples with different amounts of protons and Mn atoms are considered, including the more symmetric case (12Mn8H). [b] Muon positions extremely close to a H atom, not physically meaningful.

obtained from the two-site model are equivalent to those obtained from the one-site model, but the former distinguish the line width of muons in 8a and 16c sites ($\Delta_1 = 0.15\ \mu s^{-1}$ and 13% of $\Delta_2 = 0.35\ \mu s^{-1}$).

To understand the Δ value of $LiMn_2O_4$ at high temperature in a one-site model ($\Delta = 0.12\ \mu s^{-1}$), a small amount of muons in 16c is essential, since these sites are the only ones for which Δ decreases significantly on removal of lithium (compare second and third columns of Table 2). Thus, at high temperature muons occupy the same sites with approximately the same probability as at low temperature, but the line width is narrowed due to Li^+ movement. This assumption is supported by the thermal independence of the muon fluctuation rate, which is always lower than 0.2 MHz, and hence, the mean residence time of the muon in a site is longer than the muon lifetime. On the other hand, correlation between muons and Li^+ diffusion is not very likely, since the muon fluctuation rate at high temperature is small. Results obtained from the two-site model at 400 K were $\Delta_1 = 0.097\ \mu s^{-1}$ for site 1 and 15% of muons in site 2 with $\Delta_2 = 0.25\ \mu s^{-1}$. This situation resembles Δ_{th} for partially narrowed 8a and 16c sites. However, a one-site model seems to be more suitable in this case, since it is simpler than the two-site model and its results agree better with percentages and values of calculated line width without a lithium contribution.

4.2. λ-MnO_2. In λ-MnO_2, most of the 8a Li sites are vacant. μSR spectra have parabolic shape at short times and do not change significantly with temperature. The one-site model $\Delta = 0.14\ \mu s^{-1}$ is compatible with muons mainly in 8a sites and also a very small amount in 16c sites or in some 16d Mn vacant sites. The muon fluctuation rate is larger than Δ but constant with temperature (~0.8 MHz), which suggests it is not due to muon diffusion but to the effect of Mn nuclear relaxation due to the paramagnetism of the sample, which is similar to motional narrowing. The high hop rate could be due simply to the existence of two muon sites. If this is the case, the dynamic Kubo−Toyabe function can fit well muon data with a high hop rate. Unfortunately, the fitting is quite good for both one-site dynamic and two-site static models ($\chi^2 \sim 1$). At 100 K, the two-site model line width $\Delta_1 = 0.04\ \mu s^{-1}$ is smaller than any position in the spinel lattice, and $\Delta_2 = 0.30\ \mu s^{-1}$ (14% C2) is high for the usual 16c or 16d muon sites if lithium ions are not considered, which again suggests the influence of paramagnetism of the sample on the muon depolarization. Δ_1 does not change significantly with temperature ($\Delta_1 = 0.043 \pm 0.003\ \mu s^{-1}$

in the whole temperature range), but Δ_2 decreases to 0.25 μs^{-1} and the relative amplitude of C2 is 11% at 400 K. The small amount of Li ions remaining in λ-MnO_2 may be also responsible for this muon depolarization behavior.

4.3. $Li_{1.33}Mn_{1.67}O_4$. The probability of 8a Li vacant sites in lithium-rich spinel manganese oxide must be very low. However, calculated Δ values at 16d Mn vacant sites and at 8a Li vacant are similar (see Table 2). At low temperature, static line width value obtained from the one-site model is $\Delta = 0.31\ \mu s^{-1}$. This value can be explained by assuming approximately 50% of muons are in 16d Mn vacant ($\Delta_{th} = 0.19\ \mu s^{-1}$) and the other 50% in 16c sites ($\Delta_{th} = 0.41\ \mu s^{-1}$). The quite high muon fluctuation rate ($\nu = 0.42$ MHz) could be due to the Mn relaxation as in λ-MnO_2, since it is constant with temperature. The two-site static model suggests most of the muons to be in 16d vacant sites ($\Delta_1 = 0.18\ \mu s^{-1}$) and ~25% in 16c sites ($\Delta_2 = 0.38\ \mu s^{-1}$). Differences in the percentage of muons in 16c sites between both models probably arises from muon movement or Mn−Mn spin interactions, which are not considered in the static model. In any case, the percent of muons in 16c sites is higher than that in $LiMn_2O_4$, which agrees with the higher lithium content, i.e., small amount of Li and Mn vacant sites, of this sample.

The high-temperature experimental Δ value is 0.15 μs^{-1}, which also agrees with quasi-static muons 50% in 16d and 50% in 16c sites if Li nuclei are not considered. Since ZF μSR spectra have a Gaussian shape at low time and muon fluctuation rate is thermal independent, the line width decrease should be due to a narrowing effect due to lithium diffusion. Lithium motion begins at a temperature as low as 150 K and the increase of its mobility occurs slowly with increasing temperature, since the final state arrives at $T \geq 350$ K, as can be observed in Figure 7a. According to the two-site model, $\Delta_1 = 0.06\ \mu s^{-1}$, $\Delta_2 = 0.23\ \mu s^{-1}$, and only 25% of muons are in 16c sites. Again, both line widths decrease with temperature, but muons seem to be at the same sites and with the same probability.

4.4. H^+-MnO_2. As described above, protons occupy some 96g sites, most of the 8a Li sites are vacant in H^+-MnO_2, and residual Li is preferentially located in 8a sites. Calculated Δ values tell us that muons cannot be associated with 8a tetrahedra within which are located proton-occupied 96g sites, since Δ_{th} values at those positions are too high. Moreover, the 16c sites are no longer fully equivalent sites, since the line width in those 16c sites between an H^+-occupied oxygen tetrahedron is as high as 0.72 μs^{-1}, while in 16c sites far removed from protons it is as small as in the nonprotonated sample. Table 3 shows the four different values of Δ_{th} in the more symmetric case (12Mn8H). Protons are close to 16d Mn vacant sites, and Δ_{th} for all 16d sites also varies from 0.17 μs^{-1} distant from protons to 0.22 μs^{-1} for 16d sites between two protons. The situation thus becomes very complex. The muon fluctuation rate obtained from the one-site model is constant with temperature ($\nu = 0.61 \pm 0.04$ MHz average over all the temperature range), but it is higher than for $Li_{1.33}Mn_{1.67}O_4$, which shows a relative increase of the contribution of Mn magnetic relaxation when Li nuclei are removed. However, the μSR spectra at low temperature are better reproduced by the two-component static model, which suggests muons are mainly at 8a tetrahedra or in Mn vacancy sites free of protons ($\Delta_1 = 0.16\ \mu s^{-1}$), but also in 16c sites (~38% of $\Delta_2 = 0.38\ \mu s^{-1}$). The same muon sites with similar probabilities also reproduce the line width value obtained from the one-site model at low temperature.

When the temperature increases, not only Δ_1 and Δ_2 decrease, to 0.06 and 0.27 μs^{-1}, respectively, but also the percentage of muons in site 2 decreases. Occupancy of 16c sites decreases mainly beyond 300 K, and at 400 K it is only 10%. This effect is probably be related to the loss of protons, which occurs progressively above room temperature and until 573 K.[17] The one-site model also reproduces well the experimental spectra at high temperature, and a value of 0.13 μs^{-1} is obtained at 400 K. In fact, this value is not far from those obtained for λ-MnO_2, which suggests that at high temperature muons do not "feel" the magnetic moments of protons either due to a fast proton movement or due to proton loss as water. Similarities with λ-MnO_2 suggest that the high fluctuation rate is an intrinsic property of this spinel manganese oxide, and it is not actually due to muon diffusion. These results therefore seem to show that protons diffuse in H^+-MnO_2, although more experimental data are necessary to confirm their interpretation, and to determine any complementary information on the proton dynamics at high temperature.

5. Conclusions

Two lithium manganate spinels ($LiMn_2O_4$ and $Li_{1.33}Mn_{1.67}O_4$) and their corresponding delithiated spinel phases (λ-MnO_2 and H^+-MnO_2) have been analyzed by ZF μSR. Results are comparable to those previously reported by Kaiser et al. for $Li_{1.04}Mn_{1.96}O_4$ and $Li_{0.24}Mn_{1.96}O_4$. 8a and 16d Li and Mn defect sites and 16c sites in space group $Fd\bar{3}m$ have been identified as the most probable muon sites. The relative occupancy of 16c sites is higher for lithium- or proton-containing spinels. At low temperature muon depolarization is much higher for H^+-MnO_2 than for λ-MnO_2, which is directly related to the presence of protons in the former.

Changes in muon depolarization when temperature increases from 100 to 400 K have shown the diffusion of lithium in both lithium manganese oxides. The temperature at which the diffusion rate is comparable to the muon time scale decreases from 250 to 150 K when the content of lithium increases. As muons prefer occupying the same sites as lithium, these results support the assumption of lithium diffusion through tetrahedral 16c sites. On the other hand, depolarization is constant with temperature in the sample free of lithium and proton ions, while it decreases strongly for the spinel manganese oxide containing protons, which suggests also the diffusion of the protons.

References and Notes

(1) Hunter, J. C. *J. Solid State Chem.* **1981**, *39*, 142.
(2) Shen, X. M.; Clearfield, A. J. *J. Solid State Chem.* **1986**, *64*, 270.
(3) Ooi, K.; Miyai, Y.; Katoh, S.; Maeda, H.; Abe, M. *Langmuir* **1989**, *5*, 150.
(4) Ohzuku, T.; Kitagawa, M.; Hira, T. *J. Electrochem. Soc.* **1990**, *137*, 769.
(5) Burns, G. R.; Kane, C.; Sahasrabudhe, N. In *New Developments in Ion Exchange*; Abe, M., Kataoka, T., Suzuki, T., Eds.; Kodansha and Elsevier: Tokyo, Amsterdam, 1991; p 523.
(6) Feng, Q.; Miyai, Y.; Kanoh, H.; Ooi, K. *Langmuir* **1992**, *8*, 1861.
(7) Ammundsen, B.; Burns, G. R.; Jones, D. J.; Rozière, J. *Chem. Mater.* **1995**, *7*, 2151.
(8) Ammundsen, B.; Burns, G. R.; Jones, D. J.; Rozière, J. *Chem. Mater.* **1996**, *8*, 2799.
(9) Ammundsen, B.; Jones, D. J.; Rozière, J.; Berg, H.; Tellgren, R.; Thomas, J. O. *Chem. Mater.* **1998**, *10*, 1680.
(10) Chitrakar, R.; Kanoh, H.; Miyai, Y.; Ooi, K. *Chem. Mater.* **2000**, *12*, 3151.
(11) Yamane, H.; Inoue, T.; Fujita, M.; Sano, M. *J. Power Sources* **2001**, *99*, 60.
(12) Mosbah, A.; Verbaère, A.; Tournoux, M. *Mater. Res. Bull.* **1983**, *18*, 1375.
(13) Takada, T.; Hayakawa, H.; Akiba, E.; Izumi, F.; Chakoumakos, B. C. *J. Solid State Chem.* **1997**, *130*, 74.
(14) Shimakawa, Y.; Numata, T.; Tabuchi, J. *J. Solid State Chem.* **1997**, *131*, 138.

(15) Gao, Y.; Richard, M. N.; Dahn, J. R. *J. Appl. Phys.* **1996**, *80*, 4141.
(16) Berg, H.; Kelder, E. M.; Thomas, J. O. *J. Mater. Chem.* **1999**, *9*, 427.
(17) Ammundsen, B.; Aitchison, P. B.; Burns, G. R.; Jones, D. J.; Rozière, J. *Solid State Ionics* **1997**, *97*, 269.
(18) Du Pasquier, A.; Blyr, A.; Courjal, P.; Larcher, D.; Amatucci, G.; Gérand, B.; Tarascon, J. M. *J. Electrochem. Soc.* **1999**, *146*, 428.
(19) Thomas, J. O. Presented at the 10th International Meeting on Solid State Proton Conductors, Montpellier, France, 2000.
(20) Berg, H.; Göransson, K.; Noläng, B.; Thomas, J. O. *J. Mater. Chem.* **2000**, *10*, 1437.
(21) Lee, Y. J.; Wang, F.; Grey, C. P. *J. Am. Chem. Soc.* **1998**, *120*, 12601.
(22) Kaiser, C. T.; Verhoeven, V. W. J.; Gubbens, P. C. M.; Mulder, F. M.; de Schepper, I.; Yaouanc, A.; Dalmas de Réotier, P.; Cottrell, S. P.; Kelder, E. M.; Schoonman, J. *Phys. Rev. B* **2000**, *62*, R9236.
(23) Schenck, A. In *Muon Spin Rotation spectroscopy*; Adam Hilber: Bristol, 1985.
(24) Cox, S. F. J. *J. Phys. C: Solid State Phys.* **1987**, *20*, 3187.
(25) Karlsson, E. In *Solid State Phenomena as Seen by Muons, Protons and Excited Nuclei*; Oxford University Press: New York, 1995.
(26) Dalmas de Reotier, P.; Yaouanc, A. *J. Phys.: Condens. Matter* ***1997***, *9*, 9113.
(27) *Muon Science—Muons in Physics, Chemistry and Materials*; Lee, S. L., Kilcoyne, S. H., Cywinski, R., Eds.; SUSSP/IOP Publishing: Bristol, U.K., 1999.
(28) Lord, J. S.; Williams, W. G. *Solid State Ionics* **2001**, *145*, 381.
(29) Hempelmann, R.; Soetratmo, M.; Hartmann, O.; Wäppling, R. *Solid State Ionics* **1998**, *107*, 269.
(30) Lord, J. S.; Cottrell, S. P.; Williams, W. G. *J. Phys.: Condens. Matter* **1998**, *10*, 7975.
(31) David, W. I. F.; Thackeray, M. M.; Bruce, P. G.; Goodnough, J. B. *Mater. Res. Bull.* **1984**, *19*, 99.
(32) Aitchison, P. In *Lithium Insertion and Proton Exchange in Layered and Spinel Oxides of Cobalt and Manganese*; Victoria University of Wellington: New Zealand, 1998.
(33) Wills, A. S.; Raju, N. P.; Greedan, J. E. *Chem. Mater.* **1999**, *11*, 1510.
(34) Masquelier, C.; Tabuchi, M.; Ado, K.; Kanno, R.; Kobayashi, Y.; Maki, Y.; Nakamura, O.; Goodenough, B. *J. Solid State Chem.* **1996**, *123*, 255.
(35) Greedan, J. E.; Raju, N. P.; Wills, A. S.; Morin, C.; Shaw, S. M. *Chem. Mater.* **1998**, *10*, 3058.
(36) Hayano, R. S.; Uemura, Y. J.; Imazato, J.; Nishida, N.; Yamazaki, T.; Kubo, R. *Phys. Rev. B* **1979**, *20*, 850.
(37) Ammundsen, B.; Burns, G. R.; Islam, M. S.; Kanoh, H.; Rozière, J. *J. Phys. Chem. B* **1999**, *103*, 5175.